The Relationship Between Transport Properties and Rates of Freeze-Drying of Poultry Meat

ORVILLE C. SANDALL, C. JUDSON KING, and C. R. WILKE

University of California, Berkeley, California

Controlled studies have been made of unidirectional freeze-drying of turkey meat. The results provide a test of the model of a uniformly retreating ice front. Comparisons are made with independent measurements of thermal conductivity and with the predicted effect of pressure level upon diffusivity. Variables explored include the pressure and humidity of the drying chamber, the meat surface temperature, and the grain orientation. Drying rates were measured in the presence of water vapor alone and also in the presence of 0 to 760 mm. Hg of nitrogen or helium. Nitrogen and helium runs were made both with a stagnant gas phase and with a circulating gas stream. The rates show quantitative agreement with the uniformly retreating ice front model during the removal of most of the moisture.

Freeze-drying is a relatively new food dehydration process in which the water is removed by sublimation from the frozen state. The main advantage of freeze-drying is the relative lack of irreversible changes in the food. There is little loss of flavor, aroma, and texture. The product also maintains its initial shape and dimensions (that is, little shrinkage occurs during drying), and therefore it will rehydrate easily.

Freeze-drying in recent years has assumed an increasingly important role in the production of dehydrated foods. This is evidenced by the fact that more and more freeze-dried foods are appearing on the market. However, freeze-drying is generally a slow and consequently a costly process. Good engineering design and the development of ways to increase drying rates have been hampered by a lack of fundamental information, both on the heat and mass transfer properties of the dried materials and on the relationship between these transport properties and the drying rates. There have been various controlled laboratory freeze-drying experiments reported previously (*1, 7, 9* to *11, 14, 15, 17, 21*); however, it has usually not been possible to test models of the freeze-drying process in a reliable fashion, and in no case have drying rates been related quantitatively to independently measured transport properties of foodstuffs.

This paper presents the results of an experimental study of freeze-drying under controlled and analyzable conditions. The major aim is to develop and confirm a model which relates the fundamental transport properties of the dried material to the observed drying rates. The outer breast muscle of turkey was chosen for the experiments because of the interest in poultry as a future large-scale freeze-dried product, because of the large sample size available, and because of the opportunity to study the effect of grain orientation.

Orville C. Sandall is with the University of California, Santa Barbara, California.

MODEL

In almost all freeze-drying processes for meat, the heat necessary to sublime the ice must be transferred to the frozen zone across an increasing thickness of dried material, and the water vapor generated must be transferred out across this already dried layer. This is illustrated schematically in Figure 1.

Equations representing the rates of heat and mass transfer to and from the frozen zone can be written with a

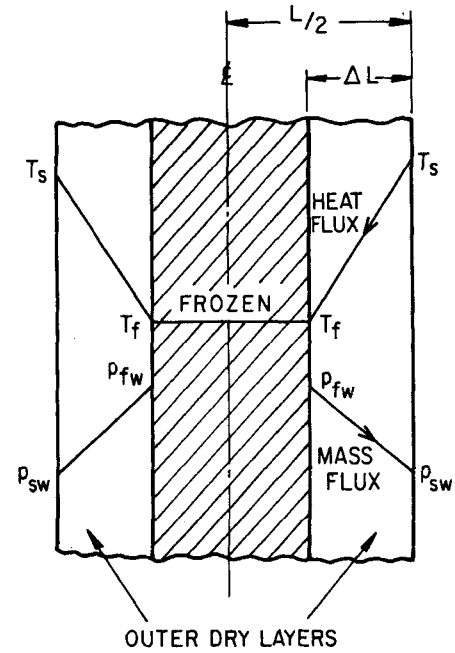

Fig. 1. Model of a uniformly retreating ice front for the freeze-drying process.

pseudo steady state in the dried layer and with uniform, one-dimensional retreat of the frozen zone assumed. For heat transfer

$$q = h\,(T_e - T_s) = \frac{k}{\Delta L}\,(T_s - T_f) \qquad (1)$$

where T_e is a measured external temperature different from T_s and h is the heat transfer coefficient external to the piece, that is, between the point with temperature T_e and the piece surface. T_s, the surface temperature of the meat, can be eliminated from Equation (1) to give

$$q = \frac{k}{\frac{k}{h} + \Delta L}\,(T_e - T_f) \qquad (2)$$

Similarly, the mass flux can be expressed as

$$N_A = \frac{k_c^*}{RT}\,(p_{sw} - p_{ew}) = \frac{D'}{RT}\,\frac{(p_{fw} - p_{sw})}{\Delta L} \qquad (3)$$

where p_{ew} is a measured external partial pressure of water and k_c^* is the mass transfer coefficient between the surface and the point with the partial pressure p_{ew}.

With p_{sw} eliminated

$$N_A = \frac{D'}{\frac{D'}{k_c^*} + \Delta L}\,\frac{1}{RT}\,(p_{fw} - p_{ew}) \qquad (4)$$

In these equations ΔL, the thickness of the dried layer, may be expressed in terms of the fraction of water remaining x, if it is assumed that complete drying occurs during the retreat of the frozen zone:

$$\Delta L = (1 - x)\,\frac{L}{2} \qquad (5)$$

Substitution of Equation (5) into Equations (2) and (4) gives

$$q = \frac{k}{\frac{k}{h} + (1 - x)\,\frac{L}{2}}\,(T_e - T_f) \qquad (6)$$

and

$$N_A = \frac{D'}{\frac{D'}{k_c^*} + (1 - x)\,\frac{L}{2}}\,\frac{(p_{fw} - p_{ew})}{RT} \qquad (7)$$

Equations (6) and (7) may be combined to give a wet-bulb relationship for freeze-drying:

$$q = \Delta H_s\, M_w\, N_A \qquad (8)$$

$$\frac{p_{fw} - p_{ew}}{T_e - T_f} = \left\{\frac{k}{D'}\,\frac{RT}{M_w}\,\frac{1}{\Delta H_s}\right\}\left\{\frac{\frac{D'}{k_c^*} + (1 - x)\,\frac{L}{2}}{\frac{k}{h} + (1 - x)\,\frac{L}{2}}\right\} \qquad (9)$$

In terms of the conditions at the piece surface the wet-bulb relationship reduces to

$$\frac{p_{fw} - p_{sw}}{T_s - T_f} = \frac{k}{D'}\,\frac{RT}{M_w}\,\frac{1}{\Delta H_s} \qquad (10)$$

It can be seen from Equation (10) that if a constant surface temperature and a constant surface partial pressure of water are maintained, then a constant ice temperature throughout the drying should result. The internal transport coefficients D' and k depend on the composition of the gas in the dried layer, and thus they are not constant throughout the dried layer, since the gas composition changes. However, the average transport coefficients, defined by integrating the transport coefficients over the thickness of the dried layer, remain constant as the drying proceeds, since composition and temperature are unique functions of the relative distance to the frozen zone. A constant ice temperature should also occur for constant T_e and p_{ew} if h and k_c^* are sufficiently large.

The drying rate can be related to the heat and mass transfer rate equations:

Heat:

$$\frac{L}{2}\,\frac{\Delta H_s}{V_w}\left(-\frac{dx}{d\theta}\right) = \left\{\frac{k}{\frac{k}{h} + (1 - x)\,\frac{L}{2}}\right\}(T_e - T_f) \qquad (11)$$

Mass:

$$\frac{L}{2}\,\frac{1}{V_w}\left(-\frac{dx}{d\theta}\right) = \left\{\frac{D'}{\frac{D'}{k_c^*} + (1 - x)\,\frac{L}{2}}\right\}\frac{M_w}{RT}\,(p_{fw} - p_{ew}) \qquad (12)$$

Equations (11) and (12) may be rearranged to forms suitable for testing drying rate data for adherence to this model and for deducing the transport coefficients from drying rate data:

$$(1 - x) = \frac{4k}{\Delta H_s}\,\frac{V_w}{L^2}\left\{\frac{T_e - T_f}{-\frac{dx}{d\theta}}\right\} - \frac{2}{L}\,\frac{k}{h} \qquad (13)$$

and

$$(1 - x) = \frac{4D'}{L^2}\,\frac{V_w}{RT}\,M_w\left\{\frac{p_{fw} - p_{ew}}{-\frac{dx}{d\theta}}\right\} - \frac{2}{L}\,\frac{D'}{k_c^*} \qquad (14)$$

A plot of $1 - x$ vs. $\left\{\frac{T_e - T_f}{-\frac{dx}{d\theta}}\right\}$ or $\left\{\frac{p_{fw} - p_{ew}}{-\frac{dx}{d\theta}}\right\}$ should be linear with a slope related to the internal transport coefficient and an intercept related to the external transport coefficient.

It is obvious that several simplifications have been made in writing these equations. For example, during drying the ice boundary will be continually progressing inward and the steady state flux equations do not strictly apply. However, an exact solution to the unsteady state, moving boundary, heat transfer problem can be obtained for the case when the ice is initially at its wet-bulb temperature (*16*). The solution is similar to the Neumann freezing problem. Calculations based on this solution indicate that the maximum error that can occur for the most extreme conditions of freeze drying is about 4% in the heat flux to the ice interface. The error in the heat flux due to neglecting the velocity of the vapor in the pores has also been estimated (*16*), and this effect on the flux is also found to be a maximum of 4%.

The model depicts all of the water present as free ice, whereas moisture adsorption experiments made in this laboratory indicate that about 12% of the initial water exerts a vapor pressure less than that of pure ice. Calculations with measured adsorption isotherms and with equilibrium of the adsorbed water with typical temperature and partial pressure gradients occurring during freeze-drying assumed indicate that the average moisture content in the dry layer is only about 3% of the initial moisture content (*16*).

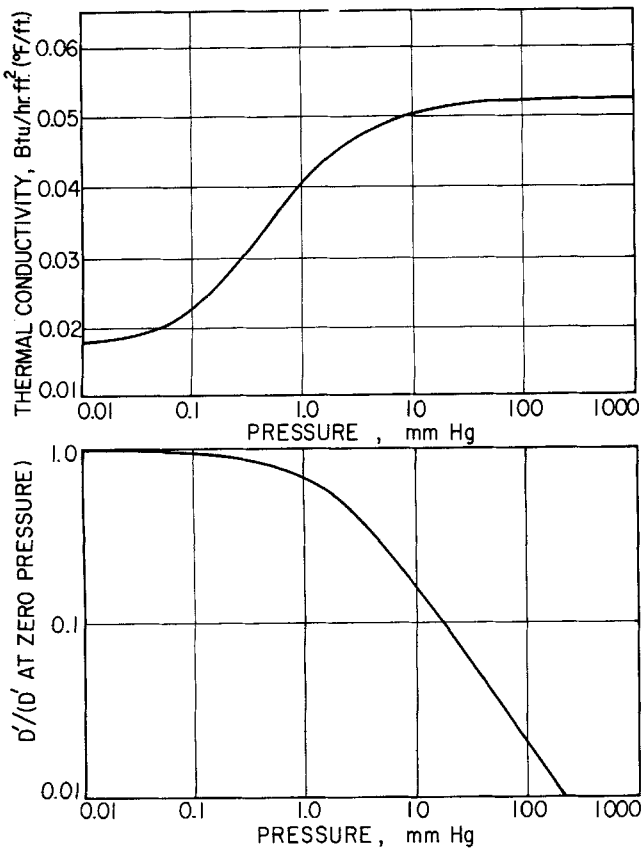

Fig. 2. *(a, top)* **Thermal conductivity of freeze-dried turkey breast in dry air (parallel to grain).** *(b, bottom)* **Mass transfer coefficient for freeze-dried turkey breast in nitrogen (parallel to grain).**

These effects are all small and thus should not significantly alter the predictions of the model.

plications for the drying rate when the heat necessary to sublime the ice must be transferred through the already dried layer.

As was stated above, the relative humidity in the dried layer during freeze-drying ranges from 100% downward, yielding a typical equilibrium average adsorbed moisture content on the order of 3% of the initial water. Triebes and King (*19*) found that the high pressure asymptote of thermal conductivity for freeze-dried turkey in air was raised by about 25% when the relative humidity was raised from 0 to 50%. The same authors show that the thermal conductivity of dry turkey is essentially independent of temperature and that there is an appreciable piece-to-piece scatter in thermal conductivity.

At the lower pressures in Figure 2*a* the mean free path of the gas is very large compared with the size of the pores, and the gas provides a negligible contribution to the overall thermal conductivity. As the pressure is increased, however, the gas phase contributes an increasing effect until at higher pressures the mean free path of the gas is very small with respect to the pore diameter, and the effective thermal conductivity is no longer a function of pressure.

Mass Transfer

In general, for binary gas mass transfer in porous media, there are four mechanisms which must be considered: (1) bulk diffusion, (2) Knudsen diffusion, (3) slip flow, and (4) Poiseuille flow. Mechanisms 1 and 2 occur because of a gradient in partial pressure, while mechanisms 3 and 4 occur because of a gradient in total pressure. For freeze-drying there will be a gradient in total pressure, since any inert gas present must be maintained stagnant within the pores. In addition, another possible mechanism for mass transport may be surface diffusion.

Wakao et al. (*20*) have proposed an equation for combined diffusion and flow in a capillary, which for diffusion through stagnant gas can be written as

$$N_A = \underbrace{\left[\frac{D_{AB}}{1-(1-m)y_A+\dfrac{D_{AB}}{D_{KA}}}\right]\frac{1}{RT}\left(-\frac{dp_A}{dz}\right)}_{\text{Knudsen and bulk diffusion}} + \underbrace{\frac{y_A}{1+\dfrac{D_{AB}}{D_{KA}}}\left[\frac{D_{KB}\pi}{4\,[y_A(m-1)+1]}+\frac{a^2P}{8\mu}\right]\frac{1}{RT}\left(-\frac{dP}{dz}\right)}_{\text{Slip}\qquad\qquad\text{Poiseuille}} \quad (15)$$

TRANSPORT PROPERTIES

Thermal Conductivity

Heat conduction in heterogeneous media such as freeze-dried materials is usually characterized by an effective thermal conductivity which accounts for heat conduction through the gas and through the solid matrix. Since the effective thermal conductivities are generally low in freeze-dried foods, and since the porosity is high, the contribution of the gas to the overall conductivity can be highly significant.

Effective thermal conductivities of freeze-dried turkey have been reported by Triebes and King (*19*). Thermal conductivities of other freeze-dried materials have been measured by Harper (*3*) and by Harper and El Sahrigi (*4*) for beef and several fruits, and by Saravacos and Pilsworth (*18*) for several low-density model food gels.

Figure 2*a* shows the thermal conductivity parallel to the grain for a sample of freeze-dried turkey in dry air as a function of pressure. These values were measured in a steady heat flux, thermopile apparatus (*19*). Similar experiments in the presence of helium showed a much higher thermal conductivity at the higher pressures. It is interesting to note that at the lower pressures freeze-dried turkey is an excellent heat insulator. This has serious im-

A somewhat different form of this equation has been obtained by Gunn (*2*) and will be discussed in a forthcoming publication. To apply such an equation to porous media, effective values of the transport coefficients should be used.

For the freeze-drying conditions of the present experiments one can make considerable simplification. Because of the limits placed on the driving forces for mass transfer and because of the relative magnitudes of the transport coefficients, the flux of water vapor through a stagnant inert gas can be represented to a good approximation by

$$N_A = \frac{D_{AB}}{1+\dfrac{D_{AB}}{D_{KA}}}\,\frac{1}{RT}\left(-\frac{dp_A}{dx}\right) \quad (16)$$

Details of this simplification are given elsewhere (*16*).

Equation (16) is represented in Figure 2*b*, where the mass transfer coefficient D' is shown as a function of total pressure. The curve has been drawn for average Knudsen and bulk diffusion coefficients which have been measured for freeze-dried turkey in this laboratory (*2*). From Figure 2*b* it can be seen that at the lowest pressures the maximum mass flux is limited by Knudsen diffusion,

whereas at higher pressures, where the mean free path of the gas becomes small compared with the size of the pores, the mass flux becomes completely bulk diffusion controlled and the flux varies inversely with pressure.

For the case of freeze-drying with no inert gas present, the limiting form of Equation (15) for $y_A = 1$, $m = 1$, and $p_A = P$ is the appropriate expression for the mass flux. However, in the absence of an inert gas, the maximum average pressure that can be used is less than 4.6 mm. Hg (triple point of water), and at these low pressures the flux of water vapor in the pores will be mainly due to Knudsen diffusion.

Limits

In an actual freeze-drying process there are limits that must be placed on the driving forces for both heat and mass transport. First there is an upper limit to the surface temperature (T_s) that can be used without thermal degradation of the dried product. This upper limit is about 60°C. for most meats (*8*). Second, there is a maximum ice vapor pressure (p_{fw}) or maximum ice temperature (T_f) above which the undried portion would no longer be frozen. It was found in the present work that this maximum ice temperature is about −5°C. for turkey because of the presence of dissolved salts.

From Figure 2 it may be seen that at low pressures D' is high but k is low. Substitution into Equation (10) shows that as T_s is increased to accelerate drying at low pressures, the limiting outer surface temperature will be reached before the limiting ice temperature. Because of the exponential nature of the ice vapor pressure relationship, $T_s - T_f$ will not change greatly even for relatively large changes in D'; consequently, an increase in k is much more effective in accelerating drying than is an increase in D'. For this reason the drying at low pressures is heat transfer controlled, and k is the important parameter for characterizing the drying rate.

At high pressures k is greater, while D' is lower than at low pressures. Substitution into Equation (10) shows that the limiting ice temperature will be reached before the limiting surface temperature. Thus the maximum possible $p_{fw} - p_{sw}$ driving force can always be made available, and the drying rate will be directly porportional to D'. An increase in k is of no use, since it would simply require that T_s be lowered further to avoid melting. Thus at high pressures the process is mass transfer controlled, and D' is the important parameter for characterizing the drying rate.

EXPERIMENTAL STUDIES

Preparation of Samples

All measurements were made on turkey breast meat (*Pectoralis superficialis,* the outer breast muscle). The samples were precooked before freezing and subsequent freeze-drying. The cooked breast muscle was sliced either parallel or perpendicular to the grain into uniform slabs of thickness ¼, ⅜, or ½ in. The slabs were then cut into 1 by 1-in. squares and a 40-gauge, butt-soldered, copper-Ideal thermocouple was threaded lengthwise into the center of each slab. The samples were frozen by placement in a Dewar flask cooled by liquid nitrogen. The edges of the samples perpendicular to the 1 by 1-in. faces were then covered with a Teflon tape, which was glued to the edges with Duco cement. The purpose of the tape was to prevent vapor flow through these sides during drying and thus to help achieve an ice front that retreated in one direction only. Details of the cooking and freezing procedures are given elsewhere (*16*).

Low-Pressure Apparatus

Low-pressure (below 100 mm. Hg) freeze-drying experiments were conducted in the apparatus shown schematically in Figure 3. For these experiments valves *A* and *B* were closed, and only that portion of the apparatus to the left of these

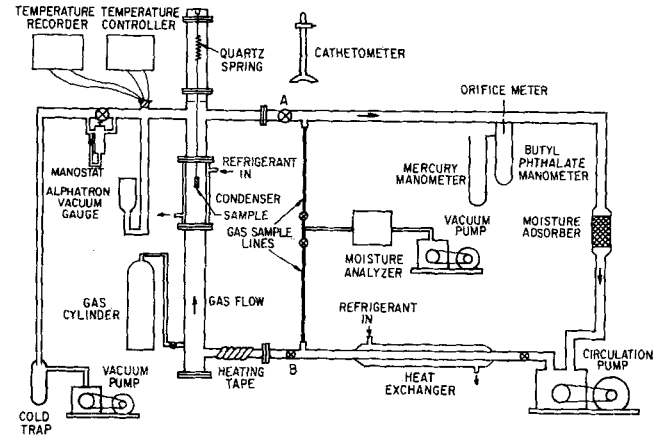

Fig. 3. Freeze-drying apparatus.

valves was used. Experiments in this apparatus covered a variety of conditions, including runs made with water vapor only in the system, drying in the presence of an inert gas atmosphere (nitrogen and helium), and a variation in controlled surface temperature from −6.7° to 60°C.

The energy necessary for the sublimation of the ice was provided by electrical surface heaters for each of the 1 by 1-in. faces. The heaters were constructed by winding 38-gauge copper magnet wire in series around a 1 by 1-in. heavy wire frame. Approximately 100 in. of wire were used for each heater, and the resistances of both heaters in a pair of heaters were matched to within 2%. A thin layer of about 1/16-in. thick porous Fiberglas insulation was glued to that surface of a heater which was in contact with the turkey. This served to even out the heat flux from the wires into the turkey surface.

The frozen samples of turkey to be dried were hung with a long dimension vertical and insulated against heat loss on the top and bottom taped edges with a ⅜-in. thickness of a styrofoam insulation. The side-taped edges were insulated with a ¼-in. thickness of a Fiberglas mat insulation. The surface heaters were attached to the frozen turkey by tying them to the turkey with a Fiberglas cord.

The weight loss during drying was followed by mounting the sample together with its heaters, insulation, and thermocouples on a quartz spring and observing the extension of the spring as a function of time. A cathetometer was employed to determine spring extensions to ± 0.05 mm.; for most runs a quartz spring with a spring constant of 0.226 g./mm. was used. Thus weight readings to within about ± 0.01 g. could be made. The presence of wires hanging from the spring affected the calibration, and for this reason the spring was calibrated in place with the wires suspended from it. The presence of the wires was found to change the spring calibration by about 7%. A material balance could be made by weighing the sample before and after drying and comparing the weight loss with that recorded from the cathetometer readings. These material balances generally agreed to about 3%.

The surface temperature of a 1 by 1-in. face was measured and controlled with a butt-soldered, 40-gauge, iron-constantan thermocouple, located between the meat surface and the Fiberglas layer. The signal from this thermocouple was read by a Brown Elektronik temperature controller with proportional plus reset action which maintained the temperature to ± 1°F. by sending an air pressure signal to a Conoflow pneumatic current controller, which in turn controlled the energy input to the surface heaters. The surface temperature could be brought up to the control temperature within about 30 sec. at the start of a run.

For drying experiments in the presence of water vapor only, the chamber pressure was regulated by adjusting a valve in the vapor exit line. The chamber pressure was controlled to within ± 20 μ of Hg at pressures below 1 mm. Hg and to within ± 100 μ Hg at pressures above 1 mm. Hg. For drying in the presence of an inert gas the pressure was controlled by bleeding the inert gas into the bottom of the drying chamber through a needle valve and by pumping the gas out of the top of the chamber through a manostat.

When an inert gas was present the water vapor generated in the process was condensed on the walls of a condenser which surrounded the sample. The condenser consisted of a copper, double-pipe heat exchanger through which an acetone refrigerant was circulated. The surface temperature of the condenser was kept constant during a run, usually at around — 50°C. This temperature was measured with a copper-Ideal thermocouple which was glued to the surface. The chamber pressure was monitored with a Model 530 NRC Alphatron vacuum gauge. Appropriate correction factors were applied for gas composition. The ice temperature as indicated by the thermocouple in the center of the sample was continuously recorded.

Convection Freeze-Drying Apparatus

Freeze-drying experiments were also made at total pressures from 50 to 760 mm. Hg, with the heat necessary to sublime the ice provided by convection from a cold, desiccated gas. These measurements were also conducted in the apparatus shown schematically in Figure 3. The gases used were nitrogen and helium. The apparatus is essentially that used for the low-pressure experiments with extra equipment added to accommodate the circulation of the gas.

At these higher pressures samples of ¼-in. thickness only were dried since the experiments generally took a longer time to complete. The samples were insulated against heat loss on the top taped edge with a ⅜-in. thickness of styrofoam insulation and on the other three taped edges with a ¼-in. thickness of Fiberglas insulation.

The turkey samples were dried by suspending them from a quartz spring into the circulating gas stream. The gas velocity through the drying chamber was maintained constant at about 2.2 ft./sec. for all runs and was measured with an orifice meter.

The gas temperature was monitored at a position about 1 in. above the sample with an iron-constantan thermocouple and was controlled by passing the gas through a refrigerated cooler and then regulating the energy input to a heating tape in order to bring the gas up to the control temperature. The same temperature controller used in the low-pressure runs was used for this purpose.

The gas humidity was controlled by passing the gas through a bed of Drierite and molecular sieve. In this manner the partial pressure of water vapor in the entering gas stream was held at about 0.05 mm. Hg. The concentration of water vapor in the gas stream entering and leaving the drying chamber was measured by withdrawing gas samples through a Meeco Model W electrolytic moisture analyzer. This also gave another check on the drying rates as determined from the cathetometer measurements. Since the moisture gain of the gas in the drying chamber was small compared with the absolute moisture level, all drying rates were based on the spring readings.

The gas pressure was controlled and measured in these experiments in the same way as in the low pressure experiments.

The drying chamber consisted of 2-in. diameter glass and copper pipe, and the gas circulation lines were constructed of 1-in. diameter copper pipe. The line connecting the drying chamber to the vacuum gauge was 1 in. in diameter; calculations show that the pressure drop in this line is negligible under the conditions of the experiments. There were about 40 in. or 20 diameters of straight pipe to establish the flow of gas after entering the drying chamber and before reaching the sample.

RESULTS

Drying Experiments with No Inert Gas

A typical weight-loss curve for drying in the presence of water vapor only is given in Figure 4, which presents data obtained for drying a ½-in. thick slab of turkey breast, where the heat and mass were transferred in a direction parallel to the grain. The conditions for the drying experiment were a controlled chamber pressure of 2.0 mm. Hg and a constant surface temperature of 30°C., as indicated and controlled by the surface thermocouple.

The final moisture content measured during a drying run was assumed to be that corresponding to equilibrium with the chamber conditions and was somewhat arbitrarily taken as zero moisture content. In several runs extended to very long drying times it was shown that this introduced negligible error in the theoretical treatment of the data. All samples were dried to complete dryness in a vacuum oven for 24 hr. at 60°C. after freeze-drying, and it was found that the equilibrium moisture content did not exceed 2 to 3% of the original moisture content.

It should be pointed out from Figure 4 that a constant ice temperature was obtained during the removal of most of the water, as is predicted from Equation (10) for the case of constant T_e and p_{ew} and no external resistances to heat and mass transfer. Since there was no inert gas in the drying chamber and since the surface temperature of the slab was controlled at a constant value, Equation (10) should be the applicable wet-bulb relationship. At the start of the run the piece temperature was low, and during approximately the first 20 min. the ice temperature rose to the steady state wet-bulb value. In the last part of the drying the temperature rose toward the surface temperature. This behavior signals the disappearance of the ice phase.

At this low pressure the drying is heat transfer controlled, and the appropriate transport parameter to characterize the drying is the thermal conductivity. The fact that the drying is heat transfer controlled can be illustrated by a consideration of the respective driving forces for heat and mass transfer. The constant ice temperature is −9.3°C., which corresponds to an equilibrium ice vapor pressure of 2.1 mm. Hg. Therefore the water vapor pressure difference which represents the driving force for mass transfer is 2.1 − 2.0 = 0.1 mm. Hg, whereas the temperature driving force is 30 − (−9.3) = 39.3°C. A comparison of these experimental driving forces with the maximum allowable driving forces for a 2 mm. Hg cham-

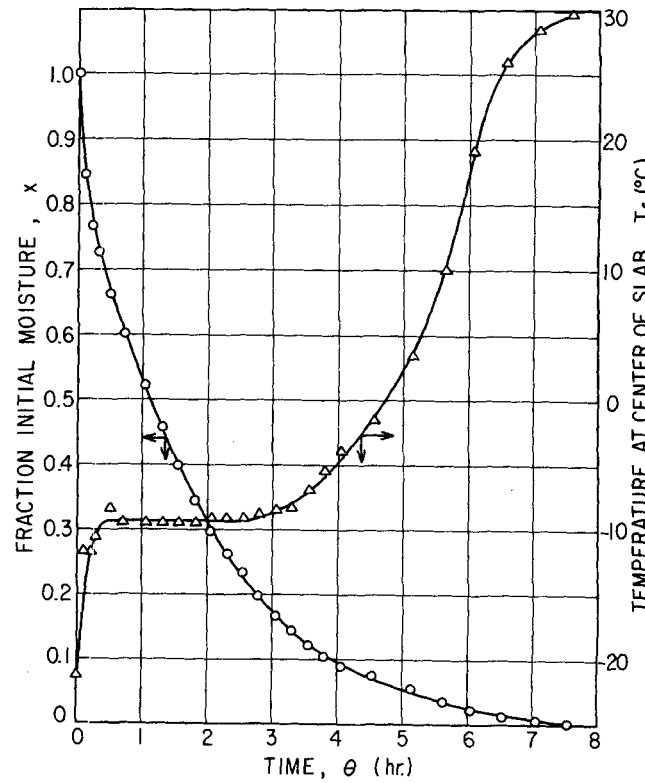

Fig. 4. Drying curve for freeze-drying in presence of water vapor only. Run 23: Sample size, 1.00 in. by 0.97 in. by 0.460 in.; surface temperature, 30°C.; chamber pressure, 2.0 mm. Hg; parallel grain orientation.

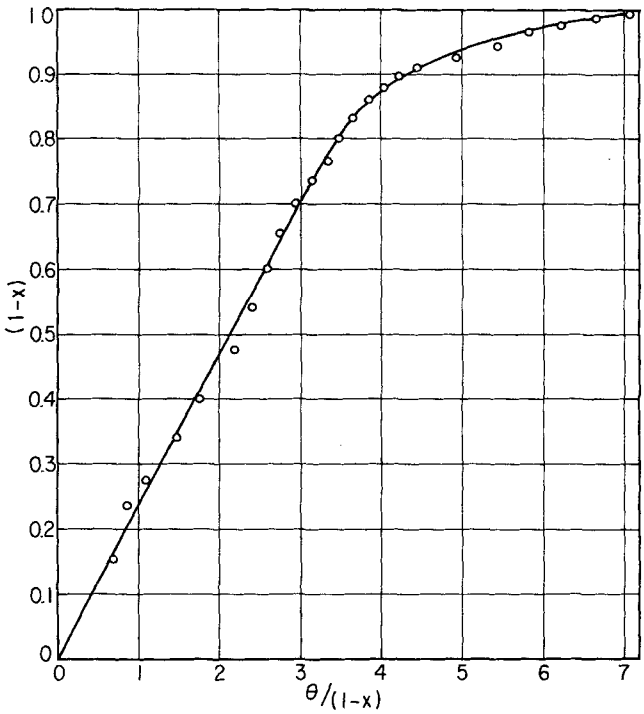

Fig. 5. Plot to test model and to determine thermal conductivity (run 23).

ber pressure shows that the drying rate is much more sensitive to k than to D'.

To allow for misplacement or poor contact of the surface thermocouple (see below) the controlled surface temperature was considered as T_e rather than T_s. Since T_e and T_f are both constant during the removal of the first 85% of the water, Equation (13) may be integrated with a constant $(T_e - T_f)$ to give another form of the rate equation which may be used to plot the weight loss data directly to obtain an indicated thermal conductivity. The appropriate boundary condition to be applied is

$$x = 1 \quad \text{at} \quad \theta = 0 \tag{17}$$

and the resultant equation is

$$(1-x) = \frac{8k\,V_w}{\Delta H_s\,L^2}\,(T_e - T_f)\left\{\frac{\theta}{1-x}\right\} - \frac{4}{L}\,\frac{k}{h} \tag{18}$$

From Equation (18) it is seen that the thermal conductivity can be determined from the slope of a plot of $(1 - x)$, the fraction of water removed, vs. $\theta/(1 - x)$, the ratio of drying time to fraction of water removed. This type of plot is shown in Figure 5 for the same run. A straight line is obtained for the removal of the first 85% of the water, indicating adherence to the model over the range of constant $T_e - T_f$.

To calculate the thermal conductivity from the slope a value of 1,200 B.t.u./lb. was postulated for ΔH_s; L was determined by micrometer measurements on the dried samples, and V_w was determined for each sample from the weight loss and micrometer measurements on the dried samples. For turkey, V_w is about 1.2 cc./g.

The method of plotting illustrated in Figure 5 indicates any misplacement or poor contact of the surface thermocouple. At pressures below about 3 mm. Hg it was quite difficult to measure the surface temperature. This problem was complicated by the desirability of measuring the surface temperature without disturbing the flow of water vapor out through the surface. Various methods to overcome this problem were tried; the most successful proved to be cutting a groove in the surface of the slab for the surface thermocouple and placing a small amount of a silicone vacuum grease on the junction of the thermocouple to promote sticking of the thermocouple to the surface. The intercept on a plot such as Figure 5 gives a heat transfer coefficient which may be thought of as a contact resistance indicating the degree of success in measuring the surface temperature. A positive intercept indicates that the groove was cut too deep, and a negative intercept (positive h) indicates poor contact between the surface and the surface thermocouple. In Figure 5 the line goes through the origin showing that the true surface temperature was measured for this run.

After a sample had been dried the thermal conductivity was measured independently, with the use of the thermopile apparatus described by Triebes and King (*19*). The pressure and composition of the gas phase in this apparatus were set the same for the thermal conductivity measurement as they had been for the drying experiment. The logarithmic mean relative humidity within the sample was set approximately the same (within 20%) relative humidity as the logarithmic mean relative humidity during drying. If the thermal conductivity is linear in relative humidity, the logarithmic mean relative humidity is the pertinent average in such an experiment. Table 1 gives a comparison between the measured thermal conductivity and the thermal conductivity as determined from the freeze-drying experiment for twenty different samples. The average absolute deviation between these two measurements is 10.4%, and the thermal conductivity from drying is on the average 8.2% higher than that measured with the thermopile apparatus. This agreement affords a striking confirmation of the retreating ice front model.

Table 2 presents the constant ice temperature and the corresponding equilibrium vapor pressure for series of runs made at different chamber pressures and at different

TABLE 1. COMPARISON OF THERMAL CONDUCTIVITY DETERMINED FROM FREEZE-DRYING EXPERIMENT WITH DIRECT MEASUREMENT

Run No.	Grain*	T_s, °C.	Gas	Pressure, mm. Hg	k measured, B.t.u./(hr.)(°F.)(ft.)	k from drying experiment, B.t.u./(hr.)(°F.)(ft.)	Deviation, %
24	Parallel	30	H_2O	0.90	0.0241	0.0223	—7.5
23	Parallel	30	H_2O	2.0	0.0378	0.0404	6.8
22	Parallel	30	H_2O	2.6	0.0490	0.0481	—1.8
55	Parallel	20	H_2O	0.90	0.0451	0.0525	16.4
39	Parallel	30	H_2O	0.90	0.0436	0.0496	13.8
18	Parallel	40	H_2O	0.99	0.0365	0.0380	4.1
38	Parallel	60	H_2O	0.90	0.0445	0.0461	3.6
33	Perpendicular	30	H_2O	0.90	0.0249	0.0251	0.6
60	Perpendicular	60	H_2O	0.90	0.0271	0.0272	0.3
44	Parallel	30	H_2O	0.90	0.0475	0.0559	17.7
35	Parallel	30	H_2O	0.90	0.0469	0.0646	37.7
25	Parallel	30	H_2O	0.90	0.0564	0.0651	15.4
20	Parallel	30	H_2O	0.90	0.0456	0.0588	28.9
43	Parallel	30	N_2	0.15	0.0326	0.0310	—4.9
40	Parallel	30	N_2	0.44	0.0448	0.0537	19.9
29	Parallel	30	N_2	0.96	0.0454	0.0454	0.0
28	Parallel	30	N_2	3.0	0.0514	0.0549	6.8
62	Parallel	4.5	N_2	6.0	0.0429	0.0493	13.0
52	Parallel	30	He	3.0	0.0464	0.0443	—4.7
57	Parallel	4.5	He	6.0	0.0579	0.0565	—2.4
						Average:	8.2%

* Orientation with respect to direction of heat and mass transfer.

Table 2. Driving Forces Required for Heat Transfer and for Mass Transfer for Freeze-Drying in Presence of Water Vapor Only

Run No.	Grain orientation with respect to direction of heat and mass transfer	p_{sw} Chamber pressure, mm. Hg	T_s Surface temp., °C.	T_f Ice temp., °C.	p_{fw} Equilibrium vapor pressure of ice corresponding to T_f, mm. Hg	$(T_s - T_f)$ Driving force for heat transfer, °C.	$(p_{fw} - p_{sw})$ Driving force for mass transfer, mm. Hg
24	Parallel	0.90	30	−17.2	1.02	47.2	0.12
23	Parallel	2.0	30	−9.2	2.10	39.2	0.10
22	Parallel	2.6	30	−6.0	2.77	36.0	0.16
55	Parallel	0.90	20	−16.2	1.11	36.2	0.21
39	Parallel	0.90	30	−16.5	1.08	46.5	0.18
18	Parallel	0.99	40	−15.3	1.20	55.3	0.21
38	Parallel	0.90	60	−16.2	1.11	76.2	0.21
33	Perpendicular	0.90	30	−14.4	1.32	44.4	0.42
60	Perpendicular	0.90	60	−7.7	2.19	67.7	1.29

surface temperatures. To a good approximation, for freeze-drying in the presence of water vapor alone the ice will assume a temperature that corresponds to an equilibrium vapor pressure equal to the chamber pressure.

At a constant chamber pressure of 0.90 mm. Hg a variation in surface temperature of 20° to 60°C. has very little effect on the ice temperature. These facts are further evidence that the process is heat transfer controlled at these low pressures.

Ice temperatures for two runs where the heat and mass were transferred in a direction perpendicular to the grain are also given in Table 1. In this case there is a more substantial water vapor pressure driving force, indicating a significantly lower permeability in a direction perpendicular to the grain than in a direction parallel to the grain. It can also be seen from Table 1 that the thermal conductivity in a direction perpendicular to the grain is also substantially less than that parallel to the grain.

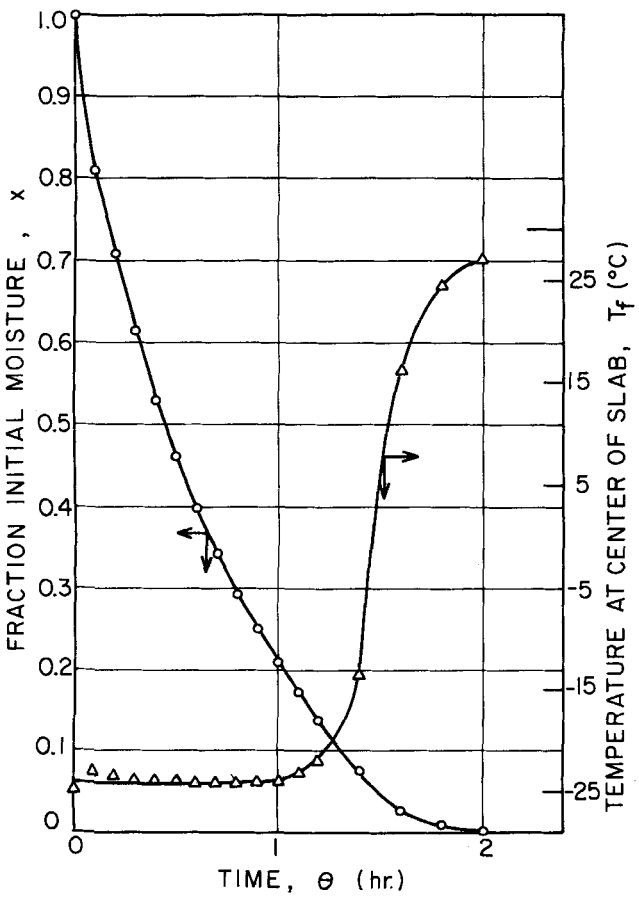

Fig. 6. Drying curve for freeze-drying in presence of nitrogen at low pressure. Run 40: Sample size, 1.00 in. by 1.00 in. by 0.359 in.; surface temperature, 30°C.; chamber pressure, 0.44 mm. Hg; condenser temperature, −49.3°C.; parallel grain orientation.

Drying in the Presence of an Inert Gas

Drying runs were made in the presence of stagnant nitrogen and helium over the pressure range 0.14 to 100 mm. Hg. At the lower pressures used, below about 6 mm. Hg, the drying is still strongly heat transfer controlled. Figure 6 shows the results of a run made with parallel grain orientation in the presence of nitrogen at a chamber pressure of 0.44 mm. Hg and a surface temperature of 30°C. Under these conditions a constant ice temperature is still obtained during the removal of most of the moisture, as was the case in runs with no inert gas. This fact can be interpreted in terms of Equation (9), the wet-bulb relationship. For a large internal mass transfer coefficient, D' and a small thermal conductivity k, the ratio $(p_{fw} - p_{ew})/(T_e - T_f)$ will be small and the changes in this ratio that are required as the drying proceeds can be made with a relatively small change in the ice temperature T_f. It should be pointed out that the total drying time for the run presented in Figure 6 is about four times smaller than for the run in Figure 4. This is accounted for in terms of the model by the fact that different sized samples were used for these runs, and for constant temperature drying the drying time is proportional to the square of the thickness. Also, since the pressure is lower for the run in Figure 6, a lower ice temperature and therefore a larger driving force for heat transfer was obtained for this run.

At higher pressures D' becomes smaller, and constant ice temperature freeze-drying no longer results. Figure 7 shows a run made at 25 mm. Hg in the presence of stagnant nitrogen. The surface temperature in this case was −6.7°C. This represents approximately the highest constant surface temperature that could be used at this pressure without thawing the frozen turkey during the initial stages of the drying. In Figure 7 the ice temperature decreases as more moisture is removed, showing the effect of the numerator in the second bracket on the right-hand side of Equation (9).

At these higher pressures, where mass transfer plays a more significant role in the drying process, an internal mass transfer coefficient may be calculated from the drying rates obtained in the freeze-drying experiment, Figure 8 shows the drying data presented in Figure 7 plotted in the manner indicated by Equation (14). In this case

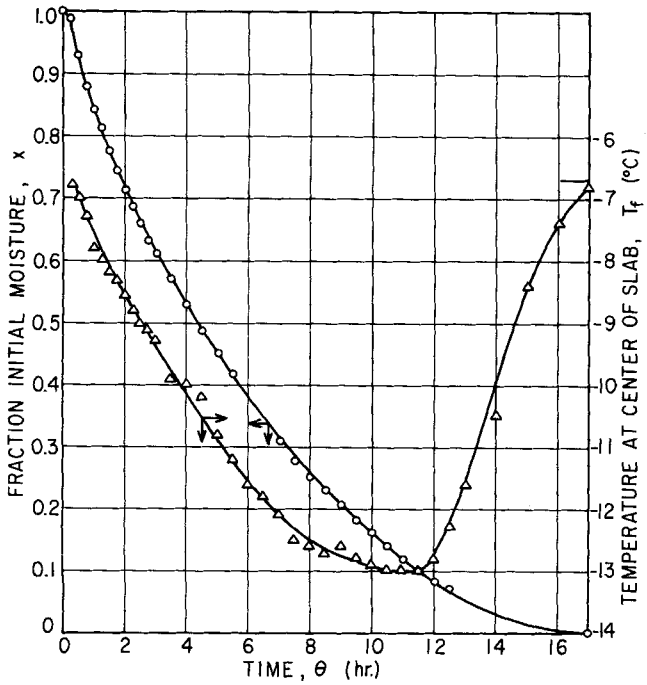

Fig. 7. Drying curve for freeze-drying in presence of nitrogen at 25 mm. Hg. Run 45: Sample size, 0.99 in. by 0.97 in. by 0.348 in.; surface temperature, —6.7°C.; chamber pressure, 25 mm. Hg (nitrogen); condenser temperature, —52.8°C.; parallel grain orientation.

p_{ew} is the equilibrium water vapor pressure at the condenser temperature. The internal mass transfer coefficient D' is determined from the slope of the line in Figure 8, and the external mass transfer coefficient k_c^* is determined from the intercept. The intercept represents the ratio of the external resistance to mass transfer to the internal resistance when the sample is completely dry. In Figure 8 this ratio is 0.76, showing that a significant fraction of the overall resistance to mass transfer lies outside the turkey.

To increase the external mass transfer coefficient and to obtain freeze-drying rates that are more a function of the properties of the turkey rather than the equipment used, the inert gas was circulated through the apparatus for runs made at higher pressures (from 50 mm. up to 1 atm.).

Figure 9 shows a run made at 760 mm. Hg of nitrogen circulated at a superficial velocity of 2.1 ft./sec. and a temperature of 20°F. In the circulation case the ice temperature rises as the drying proceeds, in contrast to the noncirculation experiments. The reason for this is that in the circulation experiments the heat required to sublime the ice was provided by the moving gas, and there was an appreciable external resistance to heat transfer to be considered in the wet-bulb relationship, Equation (9).

Values of D' and k_c^* were computed for these runs from plots similar to Figure 8. For circulation runs T_e is the controlled temperature of the gas entering the drying chamber, and p_{ew} is the measured water vapor partial pressure in the inlet gas. The use of the circulating gas system resulted in a considerable reduction in the external mass transfer resistance. At a pressure of 100 mm. Hg in nitrogen the external resistance in the circulation experiment was 50% of that in the noncirculation experiment.

The internal mass transfer coefficient D' can be related to the more basic transport coefficients, the Knudsen diffusivity and the bulk diffusivity, equating Equations (3) and (16):

$$D' = \frac{D_{AB}}{1 + \dfrac{D_{AB}}{D_{KA}}} \tag{19}$$

From any one drying experiment it is not possible to calculate both the Knudsen diffusivity and the bulk diffusivity; however, Equation (19) can be rearranged to a form

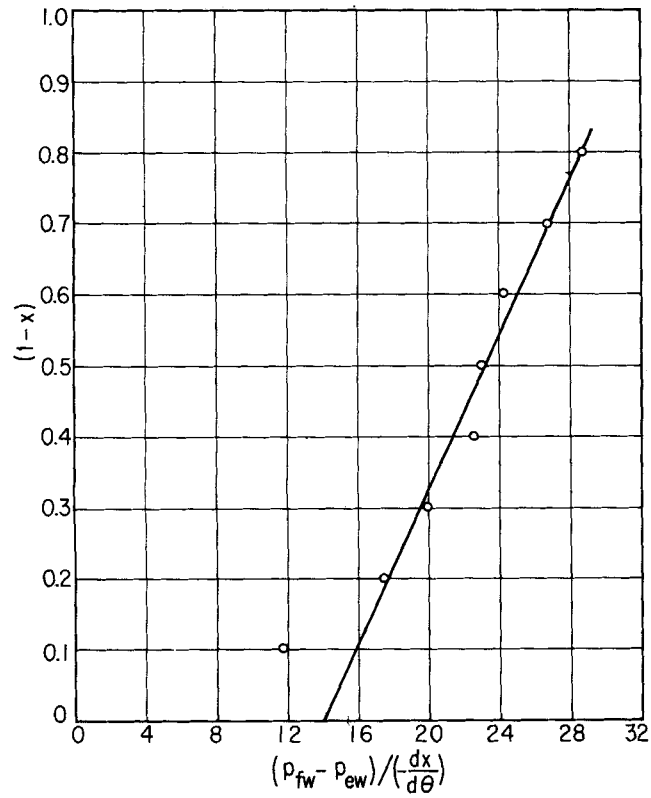

Fig. 8. Plot to determine mass transfer coefficient (run 45).

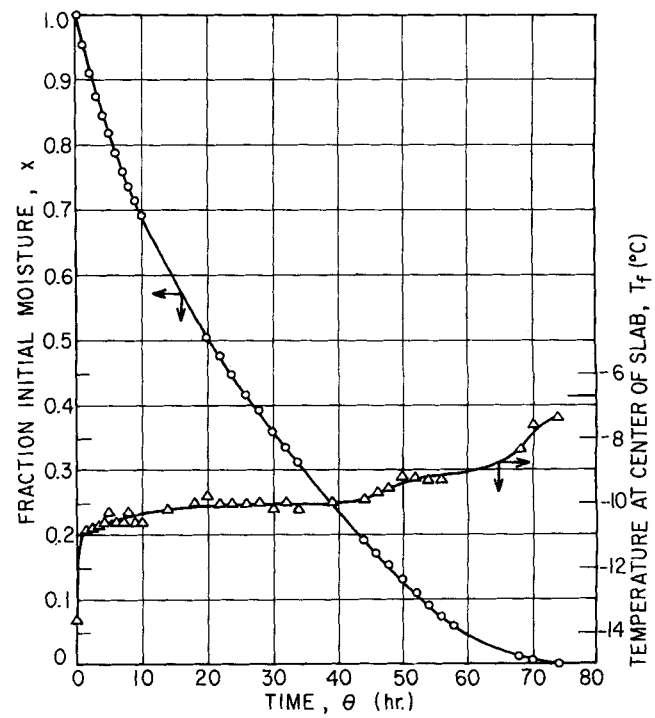

Fig. 9. Drying curve for freeze-drying in circulating nitrogen at 760 mm. Hg. Run 73: Sample size: 0.93 in. by 0.90 in. by 0.261 in.; gas temperature, —6.7°C.; chamber pressure, 760 mm. Hg; gas velocity, 2.10 ft./sec.; parallel grain orientation.

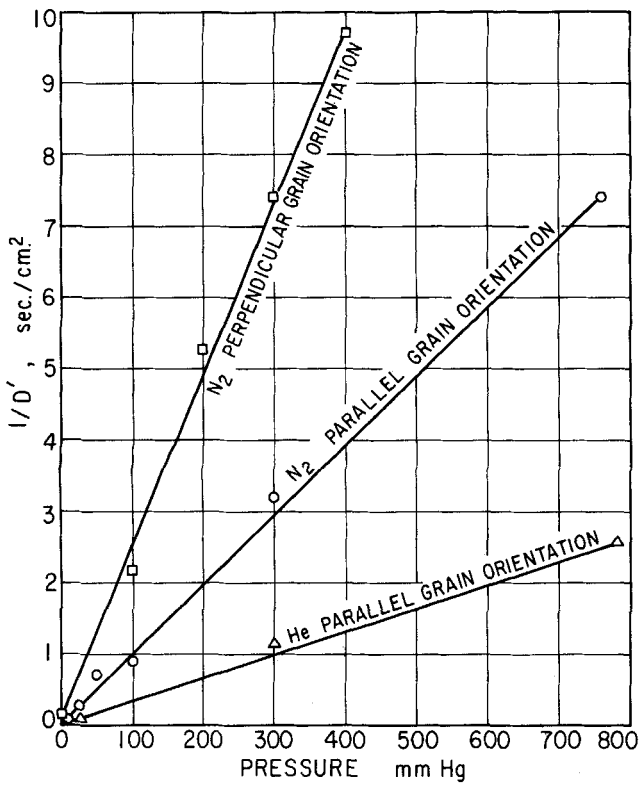

Fig. 10. Mass transfer plot for turkey No. 2.

suitable for deducing these properties from a series of experiments:

$$\frac{1}{D'} = \frac{1}{D_{KA}} + \frac{1}{D_{AB}} \tag{20}$$

Since the bulk diffusivity D_{AB} varies inversely with the pressure, it may be replaced in Equation (20) by

$$D_{AB} = \frac{D^o_{AB}}{P} \tag{21}$$

where D^o_{AB} is the bulk diffusivity at unit pressure and is a constant. Substituting Equation (21) in Equation (20), one gets

$$\frac{1}{D'} = \frac{1}{D_{KA}} + \frac{P}{D^o_{AB}} \tag{22}$$

Thus, if $1/D'$, which is determined for each freeze-drying experiment, is plotted vs. the pressure, a straight line should result, from which the slope gives the bulk diffusivity and the intercept determines the Knudsen diffusivity. This type of plot is shown in Figure 10.

Table 3 summarizes the results obtained from Figure 10 and similar experiments with samples from another turkey. The mass transfer data in this table were obtained by drying samples taken from two different birds, and it was found that a better correlation resulted if data from each turkey were treated separately. The bulk diffusivities found for freeze-dried turkey are compared in Table 3 to the diffusivity in free gas. Because of the lack of experimental diffusivity data at the average temperature (265°K.) used in the freeze-drying experiments, measured free gas diffusivities at 298°K. were corrected to 265°K. by use of the temperature dependence as predicted by the Hirschfelder–Bird–Spotz diffusivity prediction method (5). The diffusivity data of Lee and Wilke (12) were used for this purpose. A significantly lower bulk diffusivity and Knudsen coefficient were found for

Table 3. Mass Transfer Data

Turkey No.	Grain*	D_{KA}, sq. cm./sec. Helium	D_{KA}, sq. cm./sec. Nitrogen	$D_{AB}°$, (sq. cm.)(atm.)/sec. Helium	$D_{AB}°$, (sq. cm.)(atm.)/sec. Nitrogen	$D_{AB}°/(D_{AB}°)_{free\ gas}$ Helium	$D_{AB}°/(D_{AB}°)_{free\ gas}$ Nitrogen
1	Parallel	31	22	0.346	0.0901	0.466	0.440
2	Parallel	20	20	0.417	0.1345	0.562	0.656
2	Perpendicular	—	8	—	0.0549	—	0.268

* Orientation with respect to direction of mass transfer.

mass transfer in a direction perpendicular to the grain of the turkey breast than for the parallel direction.

Bulk diffusivities in porous media are usually interpreted in terms of porosity and a tortuosity factor, commonly expressed as

$$D^o_{AB} = \frac{\phi}{t^2} (D^o_{AB})_{\text{free gas}} \tag{23}$$

It is reasonable to expect that there would be a significantly higher tortuosity factor for diffusion in a direction perpendicular to the grain, and this would account for the lower diffusivity obtained.

It should be pointed out that a straight line was obtained in Figure 10 as predicted by the theory. Since the theory does not take into account any surface diffusion effects, this tends to discount any notion that surface diffusion plays a significant role in freeze-drying. If surface diffusion were important its effects should show up at high pressures where gas phase diffusion is a relatively slow process.

Terminal Drying Rates

For all runs the retreating ice front model served to describe the drying rates during the removal of the first 75 to 90% of the water. The remainder of the moisture was removed more slowly than predicted, and although the amount of water involved was small, the contribution to the total drying time was highly significant. For example, the uniformly retreating ice front model predicts a time of 4.3 hr. for complete drying in the run shown in Figures 4 and 5, whereas in reality 7.6 hr. were required to remove 98% of the initial moisture.

One possibility is that the slower rate is attributable to the removal of adsorbed or bound water; however, calculations show that the dried layer should contain only 2 to 4% of its initial moisture if equilibrium is achieved in this region after the retreat of the ice front.

Another possibility is a nonuniform retreat of the ice front. Because the thermal conductivity of the frozen turkey is twenty to fifty times higher than that of the dried layer (13), T_f and p_{fw} should be uniform at all points in the frozen zone, even if there are local variations in the thermal conductivity of the dried layer. Hence the rate of retreat of the ice front at any position must depend on the local values of D'. If D' is nonuniform, then the retreat of the ice front will be nonuniform.

Approximate calculations show that a nonplanar ice front should have only a small effect on the predictions of the uniform retreat model as long as the dried regions on either side of the slab have not met in the center at any point. Once the dried regions have met in the center over an appreciable portion of the slab, the predicted drying rates will decrease substantially. This effect may account for much of the slowing in rate observed during the removal of the last 10 to 25% of the moisture.

Approximate calculations do show that the drying rate with a nonuniform ice front should be slightly greater

than that with a planar front. This effect may account partially for the values of k obtained from the drying runs being on the average 8% greater than the measured values shown in Table 1.

Drying Rates vs. Pressure

The results shown in Figure 10 and the thermal conductivities reported by Triebes and King (*19*) may be used to predict rates of drying in the presence of various inert gases at various pressure levels. Figure 11 shows predicted drying rates in the presence of nitrogen and helium for specimens with parallel and perpendicular grain orientation. The rates are compared with those for parallel grain orientation with no inert present, for samples with the same L and x. p_{sw} is held at 0.1 mm. Hg; T_s is held at 60°C. or T_f is held at −5°C., depending upon which limit is reached first. The curves are based on the data for samples 1 and 2 in Figures 3 and 4 of reference *19* and on the parallel grain data for turkey No. 1 and the perpendicular grain data for turkey No. 2 in Figure 10 of this paper. The rates apply to the portion of drying obeying the simple model and will also apply to total drying times if one assumes that the tail of the drying curve is similar at all conditions.

The discontinuity in slope of each curve in Figure 11 corresponds to the transition from heat transfer control to mass transfer control and occurs at 7 to 17 mm. Hg. At pressures below the transition the limiting T_s is reached before the limiting T_f and the drying is heat transfer controlled. The rate increases as the pressure is raised above zero, since k increases with pressure. The increase in rate tapers off at a lower pressure for nitrogen than for helium, since the high pressure asymptote of k is reached at a lower pressure for nitrogen than for helium. For parallel grain orientation the rate actually decreases slightly above 4 mm. Hg of nitrogen pressure; this results from the increase in T_f (and decrease in $T_s - T_f$) caused by the increased mass transfer resistance.

Above the transition pressure the limiting T_f is reached before the limiting T_s. Since $p_{fw} - p_{sw}$ is now constant and D' decreases as pressure increases, the rate must decrease as pressure increases. When $1/D_{KA}$ becomes negligible in Equation (22), the rate will vary inversely as the pressure. At 1 atm. the relative rate is 0.06 for the case of helium and parallel grain orientation and is lower for the other three cases.

From Figure 11 it may be seen that the drying rate can be doubled over the value with no inert for parallel orientation by operating with 14 mm. Hg of helium, while the maximum increase with nitrogen is 20% at 2 to 7 mm. Hg. With perpendicular grain orientation the rate can be made three times greater at 17 mm. Hg of helium than with no inert and can be doubled with 9 mm. Hg of nitrogen.

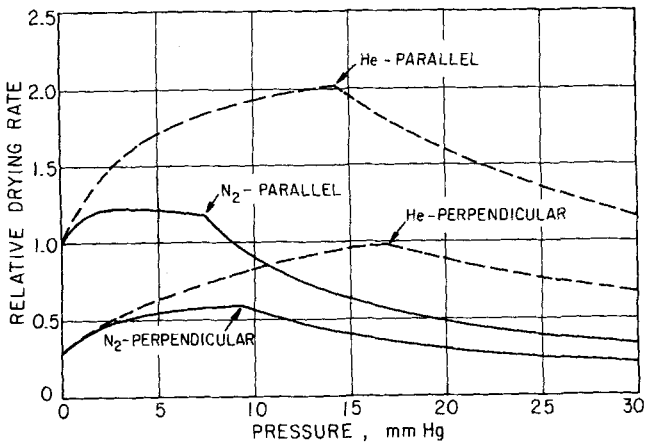

Fig. 11. Influence of pressure level and nature of inert gas upon drying rate.

These increases in rate are predicted by the model and have been confirmed by the experimental drying measurements reported in this work. Kan and de Winter (*6*) have also confirmed the rate accelerating effect of 4 to 7 mm. Hg of helium in pilot-scale studies of the freeze-drying of shrimp and peaches. Clearly, the variation of rates with inert gas pressure shown in Figure 11 has important process implications.

ACKNOWLEDGMENT

This study was carried out as part of U.S. Department of Agriculture Research and Service Contract, No. 12-14-100-7713(74).

NOTATION

a = effective pore radius
D_{AB} = binary bulk diffusivity for mixture of A and B
D_K = Knudsen diffusivity
D' = effective internal mass transfer coefficient
h = external heat transfer coefficient
ΔH_s = latent heat of sublimation for ice
k = thermal conductivity of dried layer
k_c^* = external mass transfer coefficient, allowing for effect of high concentration level
L = thickness of slab being dried from both sides
ΔL = thickness of dried layer
m = $(M_A/M_B)^{1/2}$
M = molecular weight
N_A = molar flux component A
p = partial pressure
P = total pressure
q = heat flux
R = gas constant
t = tortuosity
T = temperature
V_w = volume of food occupied by unit weight of water, initially
x = fraction of initial water still present in piece
y = mole fraction
z = distance in direction of heat flow or mass transfer
μ = viscosity (dynamic)
θ = time since start of drying
ϕ = porosity

Subscripts

A = component A
B = component B
e = external
f = frozen zone
s = outer surface of piece
w = water

LITERATURE CITED

1. Ginnette, L. F., R. P. Graham, and A. I. Morgan, Jr., *Natl. Symp. Vacuum Technol. Trans.*, **5**, 268 (1958).
2. Gunn, R. D., personal communication, Univ. California, Berkeley.
3. Harper, J. C., *A.I.Ch.E. J.*, **8**, 298 (1962).
4. ———, and A. F. El Sahrigi, *Ind. Eng. Chem. Fundamentals*, **3**, 318 (1964).
5. Hirschfelder, J. O., R. B. Bird, and E. L. Spotz, *Trans. Am. Soc. Mech. Engrs.*, **71**, 927 (1949).
6. Kan, B., and F. de Winter, paper presented at Inst. Food Tech. Mtg., Portland, Ore. (1966).
7. Kessler, H. G., *Chem. Ing. Tech.*, **34**, 163 (1962).
8. Klose, A. A., and H. S. Olcott, in "Food Dehydration," W. B. van Arsdel and M. J. Copley, ed., Avi, Westport, Conn. (1964).
9. Lambert, J. B., and W. R. Marshall, Jr., in "Freeze-Drying

of Foods," F. R. Fisher, ed., Natl. Acad. Sci.–Natl. Res. Council, Washington, D. C. (1962).
10. Larson, R. W., Ph.D. thesis, Univ. Illinois, Urbana (1962).
11. Lewin, L. M., and R. I. Mateles, *Food Technol.*, **16**, 94 (1962).
12. Lee, C. Y., and C. R. Wilke, *Ind. Eng. Chem.*, **46**, 2381 (1954).
13. Lenz, C. P., *Food Technol.*, **15**, 243 (1961).
14. Lusk, Graham, Marcus Karel, and S. A. Goldblith, *ibid.*, **18**, 1625 (1964).
15. Peck, R. E., R. A. Moraine, and D. N. Smith, Contract Res. Rept., QM Food Container Inst. Armed Forces, Contract No. DA 19-129-QM-1349, A-329, Rept. 4, final (Jan. 14, 1960).
16. Sandall, O. C., Ph.D. thesis, Univ. California, Berkeley (1966).
17. Saravacos, G. D., *Food Technol.*, **19**, 625 (1965).
18. ———, and M. N. Pilsworth, Jr., *J. Food Sci.*, **30**, 778 (1965).
19. Triebes, T. A., and C. J. King, *Ind. Eng. Chem. Process Design Develop.*, **5**, 430 (1966).
20. Wakao, Noriaki, Seiya Otani, and J. M. Smith, *A.I.Ch.E. J.*, **11**, 435, 439 (1965).
21. Zamzow, W. H., and W. R. Marshall, Jr., *Chem. Eng. Progr.*, **48**, 21 (1952).

Manuscript received August 2, 1966; revision received September 23, 1966; paper accepted September 23, 1966. Paper presented at A.I.Ch.E. Detroit meeting.

Flow Work Exchanger

CHEN-YEN CHENG, SING-WANG CHENG, and LIANG-TSENG FAN

Kansas State University, Manhattan, Kansas

In a high-pressure process, feed streams are continually pressurized and product streams are continually depressurized. A flow work exchanger offers an efficient and economical scheme for simultaneously pressurizing a fluid stream and depressurizing a substantially equivalent volume of another fluid stream. Its applicability is however limited to fluids under condensed state. A flow work exchanger uses a displacement vessel to form a closed loop with a processing system. The displacement vessel is alternately filled by a low-pressure feed and a high-pressure product, both pressurized and depressurized, respectively, by substantially nonflow processes. The pressurized feed is pushed into the processing system by the high-pressure product stream and the depressurized product stream is pushed out of the displacement vessel by the low-pressure feed stream. The application of a flow work exchanger is illustrated by means of several high-pressure processes and the direct and indirect advantages obtainable are described.

Many physical and chemical processes are carried out under high pressure. A reverse osmosis process (*1* to *5*), a freezing process based on high-pressure inversion of the order of melting points (*6*), manufacture of phenol by the hydrolysis of chlorobenzene (*7*), and hydrogenation of oil and coal (*8*) are some of the typical high-pressure processes in which at least part of the reactants and at least part of the products form condensed fluid streams. In the following discussions a condensed fluid will be used to mean any substance under condensed state that has sufficient fluidity to be handled by a pump; it may be a liquid, a slurry, or a paste.

The disadvantages of the conventional schemes of flow pressurization can be attributed to the following reasons:

1. The magnitude of the shaft work involved in a high-pressure pump or a turbine is high. The energy loss in a pumping operation increases with the magnitude of the shaft work. Therefore, both the reduction of the magnitude of shaft work and the improvement of pumping efficiency are important to the reduction of energy loss in a pumping operation. Similar arguments also apply to a depressurization operation.
2. Pumping efficiency is low. The efficiency of a centrifugal pump is usually less than 80% and the efficiency of a positive displacement pump is usually less than 90%.
3. Due to the large amount of shaft work involved, large machine members and large driving mechanisms are required. Due to the large pressure differential involved, elaborate finishing and packing are required in manufacture, which leads to high equipment costs.

A flow work exchanger herein described applies to a simultaneous pressurization of a condensed fluid *A* and depressurization of a condensed fluid *B*. The *A* and *B* fluids are pressurized and depressurized, respectively, by substantially nonflow processes. The movements of the fluids are conducted against small pressure differentials and thus $\Delta(PV)$ values for the movements of fluids are small and the shaft work is greatly reduced. This scheme of flow work exchange was first introduced by Cheng and Cheng in connection with their "freezing process which is based on the high-pressure inversion in the order of melting points" (*6*).

A flow work exchanger can exchange flow work between substantially equivalent volumes of two condensed fluids. Thus, high-pressure processes are classified into two types. Type A: A process in which the sum of the volumes of the high-pressure products in the condensed state is less than the sum of the volumes of the low-pressure feeds in the condensed state. Type B: A process in which the sum of the volumes of the high-pressure products in the condensed state is greater than the sum of the volumes of the low-pressure feeds in the condensed state.

The excess volumes will be referred to as the excess volume of feed and excess volume of product, respectively. The excess volume of feed and the excess volume of product have to be pressurized and depressurized, respectively, conventionally.

The optimal operating condition of a high-pressure process is greatly influenced by the efficiencies of the pressurization and depressurization operations. In addition to the immediate cost reduction obtainable by the adoption of flow work exchangers in a process where the operating condition is substantially left unaltered, cost reduction can also be realized by operating the process under the new optimal operating condition. This further cost reduction may be very significant in many cases.